

Geophysical Research Letters

Supporting Information for

Quantifying the Contribution of Ocean Mesoscale Eddies to Low Oxygen Extreme Events.

Jamie Atkins^{1,2}, Oliver Andrews², Ivy Frenger³

¹College of Life and Environmental Sciences, University of Exeter, Exeter, UK. ²School of Geographical Sciences, University of Bristol, Bristol, UK. ³GEOMAR Helmholtz Centre for Ocean Research Kiel, Kiel, Germany.

Contents of this file

Text S1 to S4
Figures S1 to S4

Additional Supporting Information (Files uploaded separately)

Arrays of data used to create all figures.

Introduction

We provide supporting information including four additional figures and text which complement the main findings in the main manuscript.

Figure data is processed and visualised predominantly using Python libraries including, xarray, Matplotlib, Cartopy, cmocean, netCDF4, and NumPy, as well as some processing in Matlab.

Also uploaded separately are NetCDF files and NumPy arrays of data used to create figures in the main manuscript text and supporting information.

Text S1.

Supplementary methods: We identify mesoscale eddies by employing a tracking algorithm based on the Oliver et al. (2015) implementation of the Chelton, Schlax, et al. (2011) satellite observation eddy tracking algorithm. Eddies are detected as closed contours of Sea Surface Height (SSH) anomalies from spatially high-pass filtered (20° longitude \times 10° latitude) daily SSH fields. CEs and ACEs are distinguished by their impression on SSH (CEs depress SSH, whilst ACEs elevate it). In a second step, detected features are assigned to eddy-tracks across space-time. Tracks originating in time-step i are generated by searching for each eddy centroid at time-steps $i + 1$, $i + 2$... and so on, which lie within the distance of an adaptive search ellipsoid. To test the performance of our implementation of the tracking strategy, we applied the algorithm to satellite observational data, following Chelton, Schlax, et al. (2011), and found good agreement between our version and the original Chelton, Schlax, et al. (2011) results, both in the spatial distribution and absolute counts of eddy genesis (not shown).

Physical validation: Validation of the FREEGLORYS2V4 eddy field is achieved by comparison against the eddy field based on the gridded (0.25° horizontal spacing) SSH satellite observational product distributed by the Copernicus Marine Environment Monitoring Service (CMEMS) (previously AVISO) (Pujol & Mertz, 2020). Here, the same methodology, described in Section 2 and in detail above, is used to produce an eddy field from the provided observed SSH data. The frequency distribution of eddy lifetime matches closely between model and observations (Figure S1). Eddy amplitude sees a peak at the same value of ≈ 1.5 cm for both model and observations, though the model appears to underestimate the frequency of higher amplitude eddies. With consideration to the lateral extent of the eddies tracked, there is discrepancy between model and observations. For example, the distribution of eddy surface radius is skewed towards higher values in the model simulations (model peak frequency at ≈ 88 km vs. ≈ 55 km in observations), and this effect is naturally mirrored in the eddy area values. This is due to the physical model simulation failing to resolve the eddies at the smaller end of the mesoscale. The ability of an ocean model to resolve the mesoscale at different latitudes is governed largely by the ratio between the model horizontal grid-spacing and the latitude-dependent Rossby radius of deformation, with the former needing to be significantly lower than the latter for the smallest of mesoscale features to be resolved (Hallberg, 2013; Moreton et al., 2020). This criterion is not always met at eddy-permitting resolution, which leads to an underestimation of smaller eddies.

Text S2.

Biogeochemical validation: As part of the validation procedure for the FREEGLORYS2V4 hindcast model simulation, we show modelled mean $[O_2]$ (1992–2018), WOA18 observed mean $[O_2]$ concentrations (1955–2018), and the difference between observed and modelled values, at ≈ 200 m depth (Figure S2). Whilst the model generally reproduces OMZ locations (Figure S2a), it has some biases in focus regions relative to observations (Figure S2c). In the NEA and SEA, simulated $[O_2]$ values at ≈ 200 m depth are comparatively low relative to observations in coastal regions (up to $+60$ mmol m^{-3} observations–model difference in some areas), whilst they are generally higher in open

ocean areas. Of all EBUS regions, the NEP shows the most agreement across model and observations with differences generally within the range of $\pm \approx 10 \text{ mmol m}^{-3}$. The SEP shows higher $[\text{O}_2]$ in the model, with differences of up to $\approx -60 \text{ mmol m}^{-3}$. Model $[\text{O}_2]$ biases are generally comparable to other ocean models (e.g. Séférian et al., 2020).

Text S3.

Surface circulation: Mean sea surface circulation features across the simulation period 1992 – 2018 derived from FREEGLORYS2V4 U and V fields (Figure S3). We show surface circulation directional arrows with mean current magnitude in each focus region, underlaid with average $[\text{O}_2]$ at $\approx 200 \text{ m}$ depth. Mean sea surface currents generally exhibit westward flow (Figure S3), with eddy trajectories broadly following dominant flows (e.g. see tracks of long-lived eddies in Figure 1c).

Text S4.

O₂sat decomposition: $[\text{O}_2]$ anomaly signals of eddies originating in low $[\text{O}_2]$ waters are decomposed into constituent AOU and O₂sat components. The AOU profile is shown in the main text, while the O₂sat component is shown in Figure S4. Cold-core CEs generally show positive anomalies in O₂sat. Meanwhile, warm-core ACEs tend to exhibit negative anomalies in O₂sat. Statistically significant positive O₂sat anomalies are found in SEA CEs.

It is noted that our estimates of biological consumption in eddies are calculated indirectly from model output (i.e. Equation 1 in the main text). We advocate for publicly available ocean model products to provide key biogeochemical diagnostics such as rates of biological consumption to remove reliance on indirect estimates.

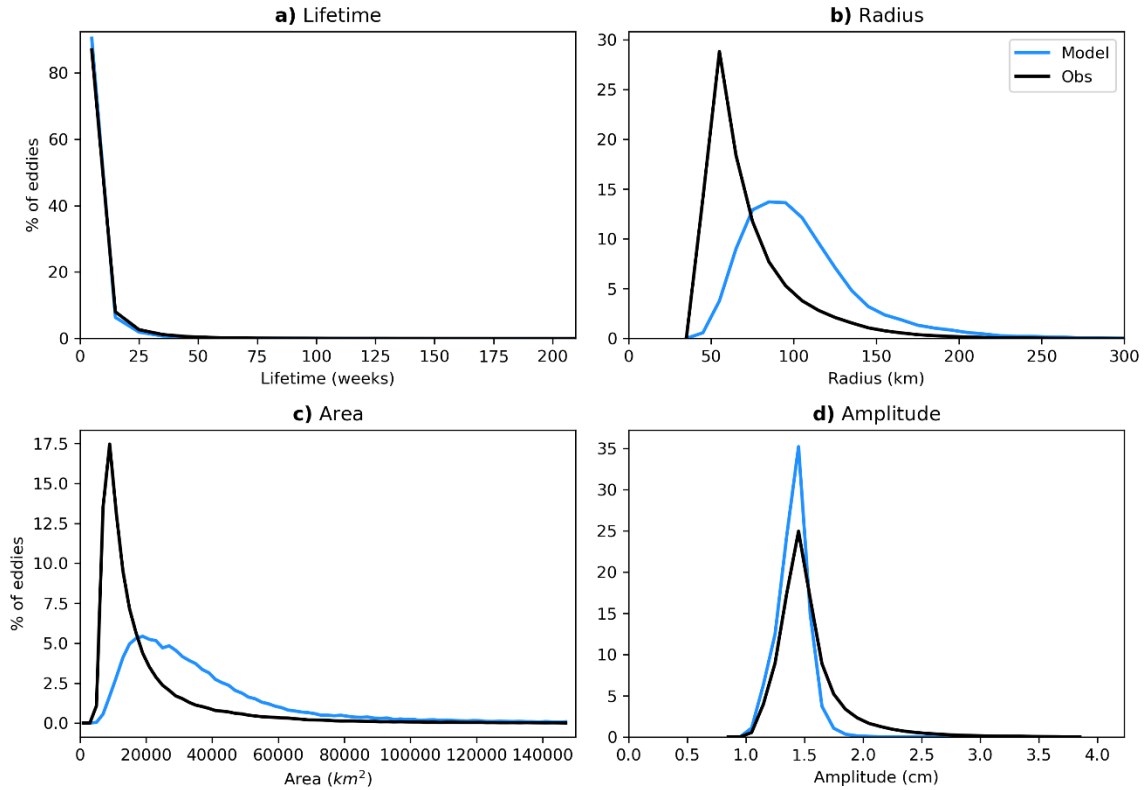


Figure S1. Frequency distributions of eddy a) lifetime, b) radius, c) area, and d) amplitude in eddies tracked (those which exceed one week lifetimes, both CEs and ACEs) in model simulations (blue line; FREEGLORYS2V4) and observations (black line; CMEMS), across the period 1993–2018 (longest overlapping period for model and observations). All eddies tracked in the four EBUS focus regions are composited to form a single distribution for each variable.

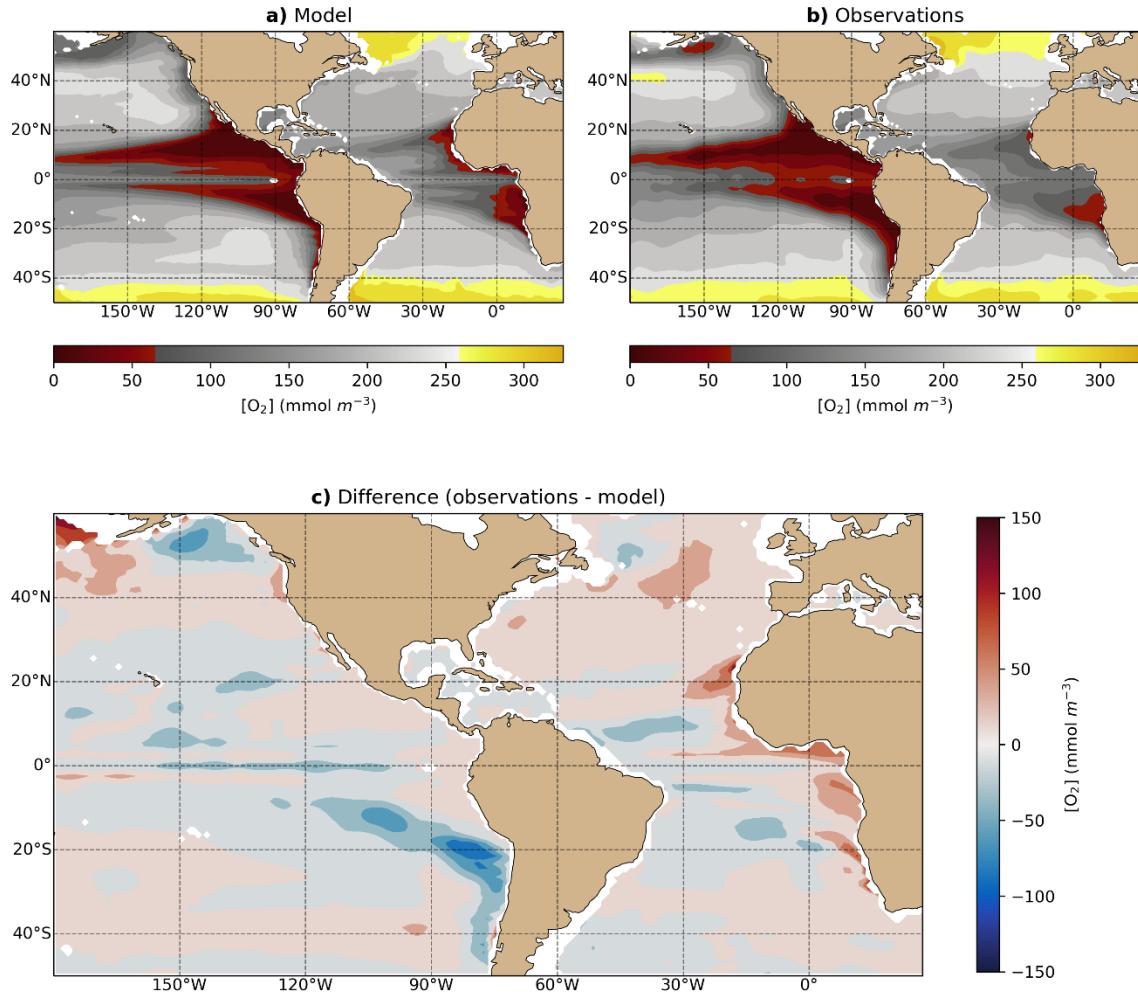


Figure S2. a) FREEBIORYS2V4 mean $[O_2]$ (across 1992–2018), b) WOA2018 mean $[O_2]$ (across 1955–2018), and c) difference between mean $[O_2]$ in WOA18 and model simulation (observations – model), at ≈ 200 m depth.

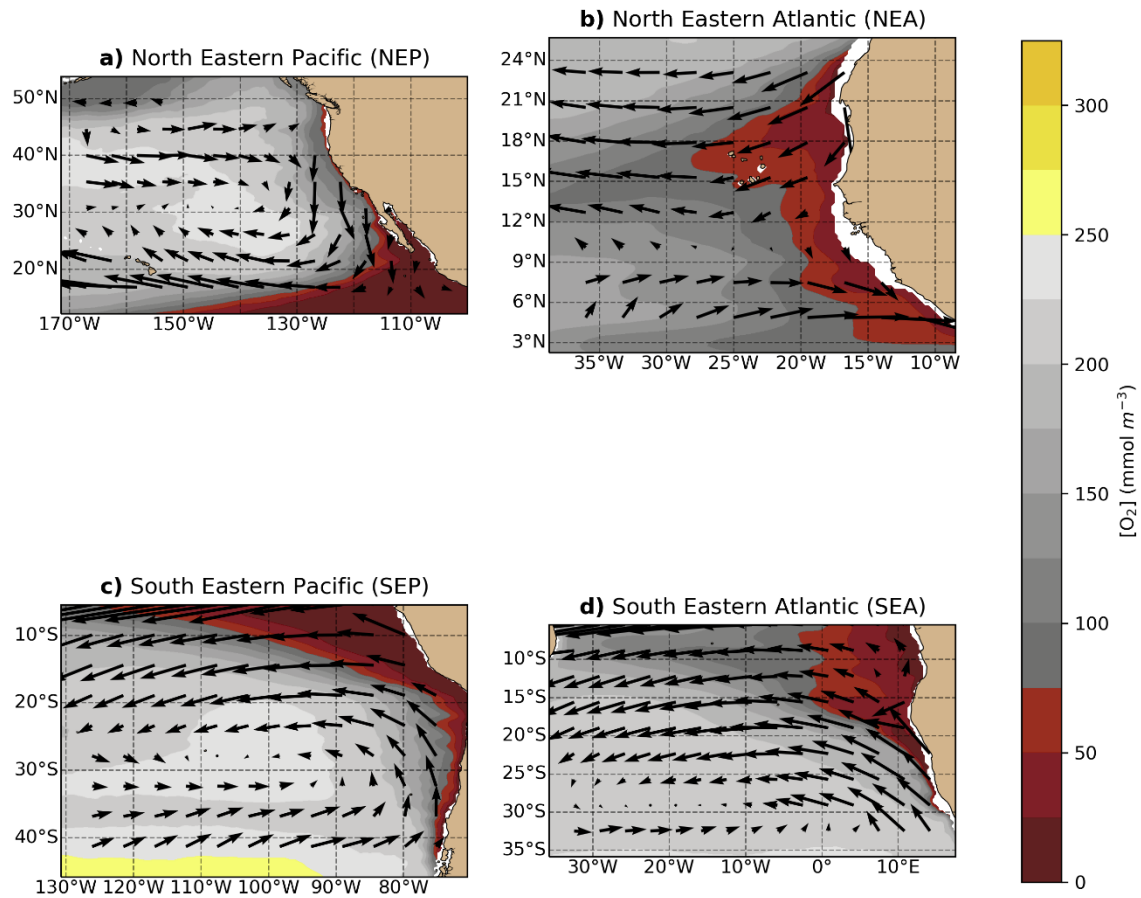


Figure S3. FREEGLORYS2V4 mean surface circulation patterns, across the simulation period 1992 – 2018, with directional arrows proportional to the relative magnitude of the flow interpolated to 10×10 grid boxes, in each focus region. Background filled contours show FREEBIORYS2V4 climatological $[\text{O}_2]$ at ≈ 200 m depth (mmol m^{-3}), across 1992 – 2018.

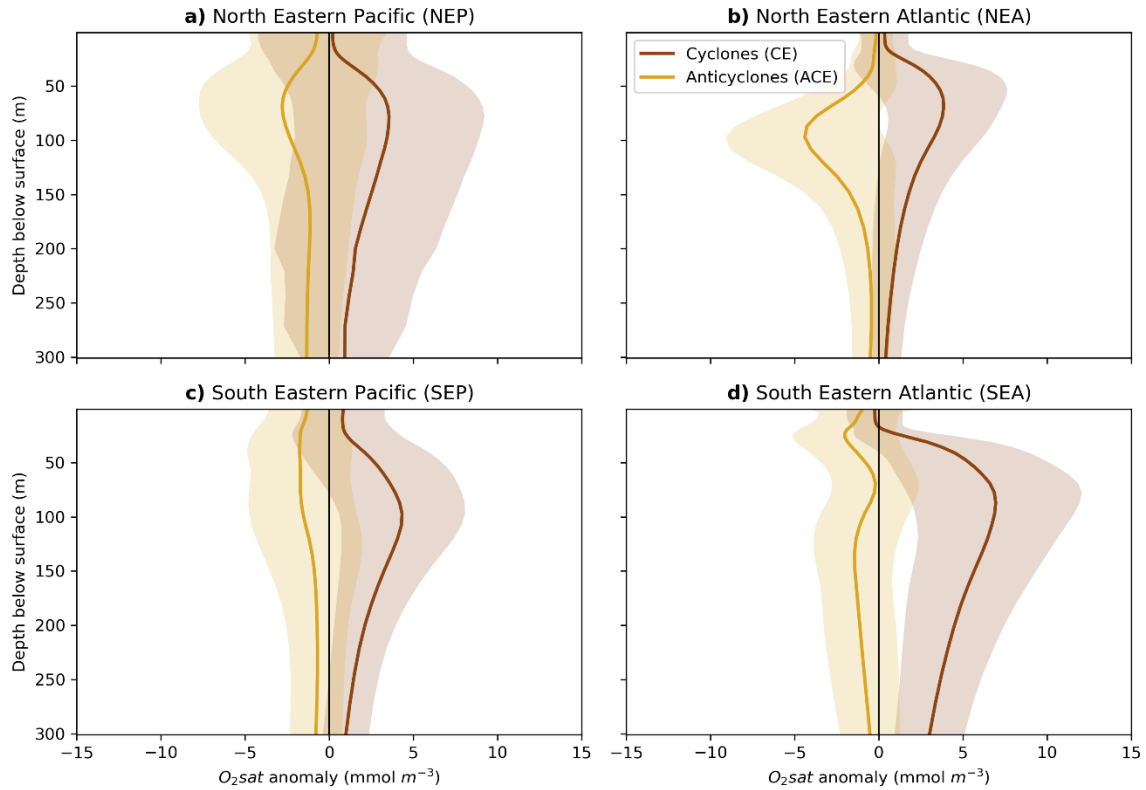


Figure S4. Composite $O_2\text{sat}$ anomaly depth profiles beneath the centroids of CEs (brown) and ACEs (yellow) which originate in low $[O_2]$ waters ($< 200 \text{ mmol m}^{-3}$) in focus regions, tracked over the period 1992–2018. Anomalies expressed relative to a non-eddy background field (see Section 2 in the main text). Solid lines are mean values of all eddies at each model depth, thereby forming a composite depth profile. Shading represents ± 1 standard deviation. Note the smaller x -axis range compared to Figure 2.